New Journal of Physics
The open access journal at the forefront of physics

Deutsche Physikalische Gesellschaft DPG IOP Institute of Physics

PAPER • OPEN ACCESS

Nonclassicality of open circuit QED systems in the deep-strong coupling regime

To cite this article: Tomohiro Shitara *et al* 2021 *New J. Phys.* **23** 103009

New Journal of Physics
The open access journal at the forefront of physics

Deutsche Physikalische Gesellschaft DPG
IOP Institute of Physics

Published in partnership with: Deutsche Physikalische Gesellschaft and the Institute of Physics

OPEN ACCESS

RECEIVED
29 June 2021

REVISED
6 September 2021

ACCEPTED FOR PUBLICATION
20 September 2021

PUBLISHED
8 October 2021

PAPER

Nonclassicality of open circuit QED systems in the deep-strong coupling regime

Tomohiro Shitara[1,*], **Motoaki Bamba**[2,3,4], **Fumiki Yoshihara**[5], **Tomoko Fuse**[5], **Sahel Ashhab**[5,6], **Kouichi Semba**[5,7] **and Kazuki Koshino**[1]

[1] College of Liberal Arts and Sciences, Tokyo Medical and Dental University, 2-8-30 Konodai, Ichikawa 272-0827, Japan
[2] The Hakubi Center for Advanced Research, Kyoto University, Yoshida-Honmachi, Sakyo-ku, Kyoto 606-8501, Japan
[3] PRESTO, Japan Science and Technology Agency, Kawaguchi 332-0012, Japan
[4] Department of Physics I, Kyoto University, Kitashirakawa Oiwake-cho, Sakyo-ku, Kyoto 606-8502, Japan
[5] National Institute of Information and Communications Technology, 4-2-1, Nukui-Kitamachi, Koganei, Tokyo 184-8795, Japan
[6] Qatar Environment and Energy Research Institute, Hamad Bin Khalifa University, Qatar Foundation, Doha, Qatar
[*] Author to whom any correspondence should be addressed.
[7] Present address: Institute for Photon Science and Technology, The University of Tokyo, Tokyo 113-0033, Japan.

E-mail: shitara.las@tmd.ac.jp

Keywords: circuit QED, nonclassicality, deep strong coupling, metrological power

Abstract

We investigate theoretically how the ground state of a qubit–resonator (Q–R) system in the deep-strong coupling (DSC) regime is affected by the coupling to an environment. We employ as a variational ansatz for the ground state of the Q–R–environment system a superposition of coherent states displaced in qubit-state-dependent directions. We show that the reduced density matrix of the Q–R system strongly depends on how the system is coupled to the environment, i.e. capacitive or inductive, because of the broken rotational symmetry of the eigenstates of the DSC system in the resonator phase space. When the resonator couples to the qubit and the environment in different ways (for instance, one is inductive and the other is capacitive), the system is almost unaffected by the resonator–waveguide (R–W) coupling. In contrast, when the two couplings are of the same type (for instance, both are inductive), by increasing the R–W coupling strength, the average number of virtual photons increases and the quantum superposition realized in the Q–R entangled ground state is partially degraded. Since the superposition becomes more fragile with increasing the Q–R coupling, there exists an optimal coupling strength to maximize the nonclassicality of the Q–R system.

1. Introduction

The interaction between a two-level system (qubit) and a harmonic oscillator (resonator) has been widely studied, originally as one of the simplest systems to study light–matter interaction [1, 2], and later as a platform for quantum optics [3–5] and quantum information processing [6–9]. The deep-strong coupling (DSC) regime of the qubit–resonator (Q–R) interaction, where the coupling strength g is comparable to or even larger than the transition energies of the qubit (Δ) and the resonator ($\omega_{\rm r}$), has recently been achieved using artificial atoms in superconducting circuit QED systems [10–13] and THz metamaterials coupled to the cyclotron resonance of a 2D electron gas [14], as reviewed in references [15, 16].

In the DSC regime, the ground state of the Q–R system is quite different from that for weaker coupling [17, 18]. First, it is an entangled state between qubit and resonator. Second, such a Schrödinger's cat-like state has a nonzero expectation value of the photon number, $\langle n\rangle = |g/\omega_{\rm r}|^2$. These photons are referred to as virtual photons, since the system is in the ground state and therefore the photons cannot be spontaneously emitted. Such nonclassical properties of the ground state are proposed to be useful for quantum metrology [19] and the preparation of nonclassical states of photons [20–22].

Any quantum system realized in an actual experimental setup, however, is coupled to external degrees of freedom, intentionally or unintentionally. Particularly, in a superconducting circuit QED system,

transmission lines are usually attached to the resonators and the qubits for control and measurement. A standard prescription for treating an open quantum system in the DSC regime is the Lindblad master equation in the dressed state picture [23], in which the system relaxes to the ground state of the system Hamiltonian at zero temperature. However, the master equation is based on the Born–Markov approximation, which assume that the system–environment interaction is sufficiently weak so that the system and the environment are always in a product state and the state of the environment does not change during the time evolution. When there is a nonzero interaction between the system and the environment, however, the total ground state can be entangled [24] and its reduced density matrix for the system is not necessarily the ground state of the system Hamiltonian. It is not clear to what extent the Born–Markov approximation is valid, or how robust the ground state properties of the DSC system are. In particular, the energy gap between the ground state and the first excited state becomes exponentially small as $\Delta \exp\left[-2g^2/\omega_{\rm r}^2\right]$ with increasing g [25]. So the nonclassicality of the ground state is expected to be fragile against the coupling to an environment in the DSC regime, although the average number of virtual photons is shown to be only quantitatively affected by losses [26]. By increasing g, there is a competition between two effects: the increase of virtual photons, which enhances the nonclassicality, and the exponential decrease of the energy gap ($\sim\Delta \exp\left[-2g^2/\omega_{\rm r}^2\right]$), which degrades the nonclassicality due to the increase of fragility, in any realistic setting. Because of this competition, it is not clear whether just increasing the coupling strength g is helpful to obtain the maximum nonclassicality in the presence of an environment, even at zero temperature.

In this paper, we investigate the ground state properties of an open DSC system. For this purpose, we propose a variational ground state for the enlarged Q–R–environment system, which we call the coherent variational state (CVS), by extending the qubit-state-dependent coherent state (equation (5)) to the total system including the environmental degrees of freedom. Based on the analysis with the CVS and the numerical diagonalization of the truncated total Hamiltonian, we find that the effect of the coupling to the environment strongly depends on how the system is coupled to the environment, i.e. inductively or capacitively. This strong dependence results from the fact that the ground state of the Q–R system in the DSC regime breaks rotational symmetry around the origin in the resonator phase space. When the resonator couples to the qubit and the environment in the same way (for instance, both inductively), we find that the average number of virtual photons increases, and that the quantum superposition realized in the Q–R system is partially degraded. Furthermore, the ground state superposition tends to be more fragile when the Q–R coupling g is larger, so that the nonclassicality of the resonator state, measured by the metrological power [27], is maximized at a moderate strength of the Q–R coupling. When the resonator couples to the qubit inductively and to the environment capacitively, on the other hand, we did not observe any peak of the metrological power in the parameter region that we investigated, so that enhancement in metrological power is achievable.

This paper is organized as follows. In section 2, we describe the theoretical model and present examples of superconducting circuits realizing the Hamiltonian that we analyze. In section 3, we outline the variational method based on the CVS. In section 4, by using the CVS and the numerical diagonalization, we numerically evaluate the number of virtual photons, the purity in the Q–R system, and the degree of nonclassicality measured by the metrological power. In section 5, we discuss how the coupling-type dependence arises in the DSC system. We conclude the paper in section 6. In appendix A, we describe the detailed derivation of the Hamiltonian from the circuit model. In appendix B, we discuss the relation to the spin-boson model. In appendix C, we discuss how the symmetry of the total Hamiltonian restricts the form of the CVS. In appendix D, we show that the stationary equations for the CVS can be substantially simplified by introducing a collective variable. In appendix E, we check the validity of the CVS in the inductive coupling case by comparing the result from the numerical diagonalization and perturbation theory. In appendix F, we discuss the effect of counter-rotating terms and the rotating-wave approximation (RWA) in the resonator–waveguide (R–W) coupling.

2. Model

In this section, we describe the model considered in this paper. The relationship among the system, the environment, and the total system is summarized in figure 1.

2.1. Qubit and resonator

We consider the quantum Rabi model, which is described by the Hamiltonian

$$H_{\rm S} = \omega_{\rm r} a^\dagger a + \frac{\Delta}{2}\sigma_x + g\sigma_z(a + a^\dagger). \tag{1}$$

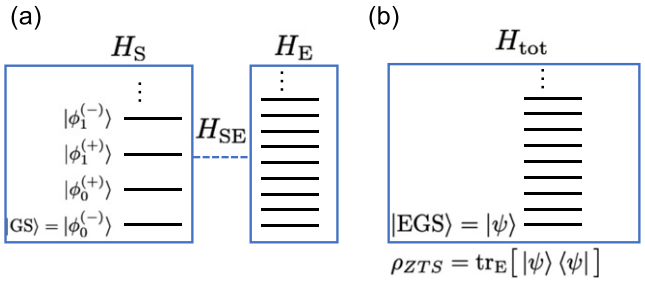

Figure 1. Energy diagrams of the qubit-resonator waveguide (Q–R–W) system. (a) The Q–R system (described by H_S) for $g > \omega_r/2$ and the environmental waveguide system (described by H_E) are coupled with H_{SE}. (b) We denote the enlarged ground state of $H_{tot} = H_S + H_E + H_{SE}$ by $|EGS\rangle = |\psi\rangle$. Its reduced matrix to the Q–R space is referred to as the zero-temperature state and is denoted by $\rho_{ZTS} = \mathrm{tr}_E\left[|\psi\rangle\langle\psi|\right]$.

Here, $a(a^\dagger)$ is the annihilation (creation) operator of a resonator photon with energy ω_r, σ_j $(j = x, y, z)$ is the Pauli operator of the qubit with transition energy $\Delta(>0)$, and g is the coupling strength between them. The Planck constant $\hbar$ is set to unity throughout this paper. Here, we assume that $X_I = a + a^\dagger$ is proportional to the flux operator, so that the Q–R coupling is inductive. When the coupling is capacitive, X_I is replaced with $X_C = (a - a^\dagger)/i$ as

$$H_S' = \omega_r a^\dagger a + \frac{\Delta}{2}\sigma_x - ig\sigma_z(a - a^\dagger), \tag{2}$$

after choosing an appropriate basis for qubit states. Both H_S and H_S' are unitary equivalent through a gauge transformation $a \leftrightarrow ia$, where the unitary operator is explicitly given by $U = \exp\left[\pm i\pi a^\dagger a/4\right]$.

We note that there is a subtlety originating from the choice of gauge in the theoretical treatment of the system [28–31]. Although the microscopic model of the circuit should possess gauge invariance, the approximation in which only two levels are retained for the qubit part of the circuit often breaks gauge invariance. Specifically, the truncated Hamiltonian depends on the choice of gauge. We do not discuss this aspect in detail here. We simply assume that the qubit and resonator are described by the quantum Rabi model. In other words, our analysis and results apply to physical systems for which the quantum Rabi Hamiltonian provides a good approximation for the low-energy physics.

When $\omega_r \gg \Delta$ or $g \gg \omega_r, \Delta$, the low-lying eigenstates of the quantum Rabi model are approximately described by [17, 18]

$$|\phi_n^{(\pm)}(\alpha)\rangle = \frac{1}{\sqrt{2}}\left(|\uparrow\rangle \otimes D(-\alpha)\,|n\rangle \pm |\downarrow\rangle \otimes D(\alpha)\,|n\rangle\right), \tag{3}$$

which is also denoted as $|\phi_n^{(\pm)}\rangle$. Here, $|\uparrow\rangle$ $(|\downarrow\rangle)$ is the qubit eigenstate corresponding to $\sigma_z = +1$ (-1), $\alpha = g/\omega_r$ is the amplitude of displacement in the resonator, and $D(\alpha) = \mathrm{e}^{\alpha a^\dagger - \alpha^* a}$ is the displacement operator. These parameter regions are referred to as the adiabatic oscillator limit [17, 32–34] or the perturbative DSC regime [16, 18], in the sense that the perturbation in terms of Δ is valid. The eigenenergy is then, up to first order in Δ/ω_r, given by

$$E_n^\pm \simeq n\omega_r - \frac{g^2}{\omega_r} \pm \frac{\Delta}{2}\langle n|D(2\alpha)|n\rangle = n\omega_r - \frac{g^2}{\omega_r} \pm \frac{\Delta \mathrm{e}^{-2\alpha^2}}{2} L_n(4\alpha^2), \tag{4}$$

where $L_n(x)$ is the Laguerre polynomial of the nth order. We note that the ground state,

$$|\mathrm{GS}\rangle = |\phi_0^{(-)}\rangle = \frac{1}{\sqrt{2}}\left(|\uparrow\rangle \otimes |-\alpha\rangle - |\downarrow\rangle \otimes |\alpha\rangle\right), \tag{5}$$

is the superposition of two coherent states displaced in opposite directions depending on the qubit state.

2.2. Coupling to the environment

The environment can be modeled by an ensemble of harmonic oscillators [35] as

$$H_E = \sum_k \omega_k b_k^\dagger b_k, \tag{6}$$

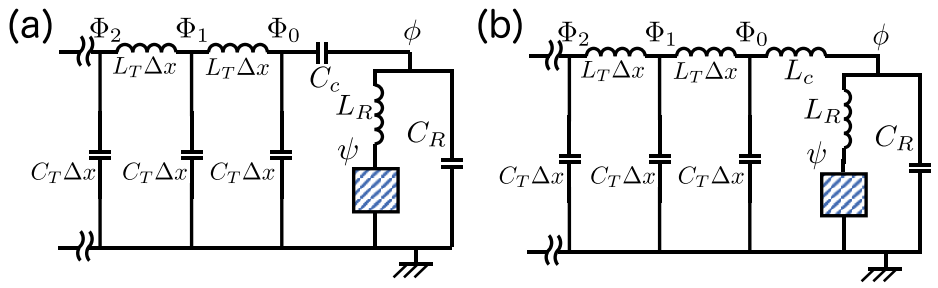

Figure 2. Circuit diagrams of a Q–R system coupled to a waveguide. The blue shaded area is an arbitrary circuit representing the qubit. The R–W coupling is mediated by (a) a capacitance C_c or (b) an inductance L_c.

where b_k ($b_k^\dagger$) is the annihilation (creation) operator of the kth mode with energy ω_k. Each mode of the environment interacts with a system operator X with strength ξ_k as

$$H_{\rm SE} = \sum_k \xi_k X (b_k + b_k^\dagger). \tag{7}$$

The total system is then described by the Hamiltonian $H_{\rm tot} = H_{\rm S} + H_{\rm E} + H_{\rm SE}$.

As a concrete model of an open DSC system, we investigate a DSC system coupled to a waveguide through the resonator (figure 2). The blue shaded area can be an arbitrary circuit constituting a qubit, such as a Cooper pair box or a flux qubit. The waveguide is coupled to the Q–R system through (a) a capacitance C_c or (b) an inductance L_c. When the interaction is mediated by an inductance (a capacitance), the operator X through which the system is coupled to the waveguide is the quadrature operator of the resonator, given as $X_{\rm I} = a + a^\dagger$ ($X_{\rm C} = (a - a^\dagger)/i$). We note that in the case of the capacitive coupling, the interaction Hamiltonian is given by $H_{\rm SE} = -\sum_k \xi_k (a - a^\dagger)(b_k - b_k^\dagger)$. This is equivalent to equation (7) under the unitary transformation $b_k \to -ib_k$. While the phase of the quadrature operator for b_k does not affect the physical result because of the gauge invariance of $H_{\rm E}$, the phase of the quadrature operator for a has the physical influence since it is used to couple the resonator to not only the waveguide but also the qubit. In the following, we always assume that the Q–R coupling is inductive, and we analyze the cases where the R–W coupling is inductive or capacitive, except for section 5, where we discuss the relativity of the coupling.

Assuming a finite length L of the waveguide, the wavenumber k of the waveguide modes is discretized as $k = n\pi/L$ ($n \in \mathbb{N}$), and the energy is given by $\omega_k = vk$, where v is the speed of microwave fields in the waveguide. The coupling constant ξ_k is given by

$$\xi_k = \xi_0 \sqrt{\frac{\omega_k}{1 + (\omega_k/\omega_{\rm cutoff})^2} \times \frac{\pi}{L}} \tag{8}$$

in both the capacitive [36] and inductive coupling case. We do not have to put the cutoff factor by hand, since it is naturally included in the Hamiltonian derived from the circuit, and the cutoff energy $\omega_{\rm cutoff}$ is determined from the circuit parameters (equations (A.26) and (A.29)). In the small frequency region ($\omega_k \ll \omega_{\rm cutoff}$), the squared coupling strength $|\xi_k|^2$ is proportional to ω_k, which corresponds to the Ohmic case in the spin-boson model (see appendix B for details).

The loss rate κ of a bare resonator photon into the waveguide is determined by the Fermi Golden rule as

$$\frac{\kappa}{2\pi} = \xi_0^2 \frac{\omega_{\rm r}}{1 + (\omega_{\rm r}/\omega_{\rm cutoff})^2}. \tag{9}$$

3. Coherent variational state

In this section, we introduce the CVS and analyze the ground state of $H_{\rm tot}$. In analogy to the approximate ground state of the quantum Rabi model (equation (5)), we define the CVS of the total system as

$$|\psi_{\rm C}(\alpha, \{\beta_k\})\rangle = \frac{1}{\sqrt{2}}(|\uparrow\rangle \otimes |-\alpha; \{-\beta_k\}\rangle - |\downarrow\rangle \otimes |\alpha; \{\beta_k\}\rangle), \tag{10}$$

where $|\alpha; \{\beta_k\}\rangle$ is the product of coherent states of the resonator and waveguide modes, satisfying $a|\alpha; \{\beta_k\}\rangle = \alpha|\alpha; \{\beta_k\}\rangle$ and $b_k|\alpha; \{\beta_k\}\rangle = \beta_k|\alpha; \{\beta_k\}\rangle$ for each k. The variational parameters for the CVS

are α and β_k's. We note that a more general form $c_0|\uparrow\rangle\otimes|\alpha;\{\beta_j\}\rangle + c_1|\downarrow\rangle\otimes|\alpha';\{\beta'_j\}\rangle$ leads to the same results as the simpler form in equation (10) due to the parity symmetry of the quantum Rabi Hamiltonian, as discussed in appendix C. We also note that the renormalization of the qubit energy and the Rabi oscillation were analyzed using a similar ansatz by performing a polaron transformation [37].

The total energy for the CVS is given by

$$\begin{aligned} E_{\rm CVS} &= \langle\psi_{\rm C}(\alpha,\{\beta_k\})|H_{\rm tot}|\psi_{\rm C}(\alpha,\{\beta_k\})\rangle \\ &= \omega_{\rm r}|\alpha|^2 - g(\alpha+\alpha^*) + \sum_k \omega_k|\beta_k|^2 \\ &\quad \pm \sum_k \xi_k(\alpha\pm\alpha^*)(\beta_k\pm\beta_k^*) - \frac{\Delta}{2}\exp\left[-2\left(|\alpha|^2+\sum_k|\beta_k|^2\right)\right], \end{aligned} \tag{11}$$

where the plus (minus) sign represents the inductive (capacitive) coupling. The approximate ground state of the total system is the CVS $|\psi_{\rm C}(\bar{\alpha},\{\bar{\beta}_k\})\rangle$, where $\bar{\alpha}$ and $\bar{\beta}_k$'s are the variational parameters that minimize the total energy $E_{\rm CVS}$. Although there are a large number of degrees of freedom due to the numerous waveguide modes, the problem can be simplified into a stationary state problem with only two unknown parameters, α and $S=\sum_k|\beta_k|^2$, as discussed in appendix D. Here, S is a collective variable for the waveguide modes, representing the total number of virtual photons in the waveguide modes.

Once $\bar{\alpha}$ and $\bar{S}=\sum_k|\bar{\beta}_k|^2$ are obtained, the reduced density operator for the system, $\rho_{\rm ZTS}={\rm tr}_{\rm E}[|\psi_{\rm C}(\bar{\alpha},\{\bar{\beta}_k\})\rangle\langle\psi_{\rm C}(\bar{\alpha},\{\bar{\beta}_k\})|]$, which we call the zero-temperature state, is completely characterized by two parameters $\bar{\alpha}$ and $C=\exp\left[-2\bar{S}\right]$. It is explicitly expressed as

$$\rho_{\rm ZTS} = \frac{1+C}{2}|\phi_0^{(-)}(\bar{\alpha})\rangle\langle\phi_0^{(-)}(\bar{\alpha})| + \frac{1-C}{2}|\phi_0^{(+)}(\bar{\alpha})\rangle\langle\phi_0^{(+)}(\bar{\alpha})|. \tag{12}$$

This equation implies that the R–W coupling has two effects. First, the displacement $\bar{\alpha}$ is modified from $\alpha=g/\omega_{\rm r}$, which means that the average number of virtual photons $|\bar{\alpha}|^2$ is changed. In fact, as we will see in section 4, the number of virtual photons increases as the R–W coupling increases. Second, $\rho_{\rm ZTS}$ includes the first excited state of $H_{\rm S}$ with a fraction $P_{\rm e}=\frac{1-C}{2}$. A similar behavior can be found in the case of a single two-level system coupled to an environment [35].

The quantity C serves as a measure of coherence, which is a real quantity within the range of $0\leqslant C\leqslant 1$. If $\bar{\beta}_k=0$ and hence $C=1$, the system is in a pure state. On the other hand, if $C=0$, the quantum superposition is completely destroyed and the reduced density matrix $\rho_{\rm S}$ is maximally mixed. When we represent $\rho_{\rm S}$ in the basis of $|\uparrow\rangle\otimes|-\bar{\alpha}\rangle$ and $|\downarrow\rangle\otimes|\bar{\alpha}\rangle$, the quantity C appears in the off-diagonal element:

$$\rho_{\rm ZTS} = \frac{1}{2}\begin{pmatrix} 1 & -C \\ -C & 1 \end{pmatrix}. \tag{13}$$

In this sense, R–W coupling reduces the coherence realized in this basis.

The purity of $\rho_{\rm ZTS}$ can be calculated as

$$\gamma = {\rm tr}[\rho_{\rm ZTS}^2] = \frac{1+C^2}{2} = \frac{1+{\rm e}^{-4\bar{S}}}{2}, \tag{14}$$

which means that the purity is a simple function of the total number of virtual photons in the waveguide, and vice versa. In this way, the analysis based on the CVS clarifies the relation between the decoherence in the Q–R system and the virtual photons in the waveguide.

As for the validity of the CVS, we note that it gives the exact ground state of the total Hamiltonian if the qubit energy Δ and the counter-rotating terms $\xi_k(ab_k+a^\dagger b_k^\dagger)$ are neglected. In reference [11], it is argued that the Q–R state $|\phi_0^{(-)}\rangle$ gives a rather accurate description of the ground state of the quantum Rabi Hamiltonian even when the qubit energy Δ is finite. Furthermore, we compare the result of CVS in the inductive coupling case with that of the numerical diagonalization for a few waveguide mode case in appendix E, and show that the CVS describes not only the virtual photons but also the nonclassical properties well in the presence of the R–W coupling. We also compare the results from the CVS and perturbation theory with an infinite number of waveguide modes, and confirm that they are in good agreement in appendix E.

4. Numerical calculations

In this section, we numerically investigate the properties of $\rho_{\rm ZTS}$ based on the CVS. We adopt the bare resonator photon loss rate κ (equation (9)) as a measure of the R–W coupling strength. The Q–R coupling

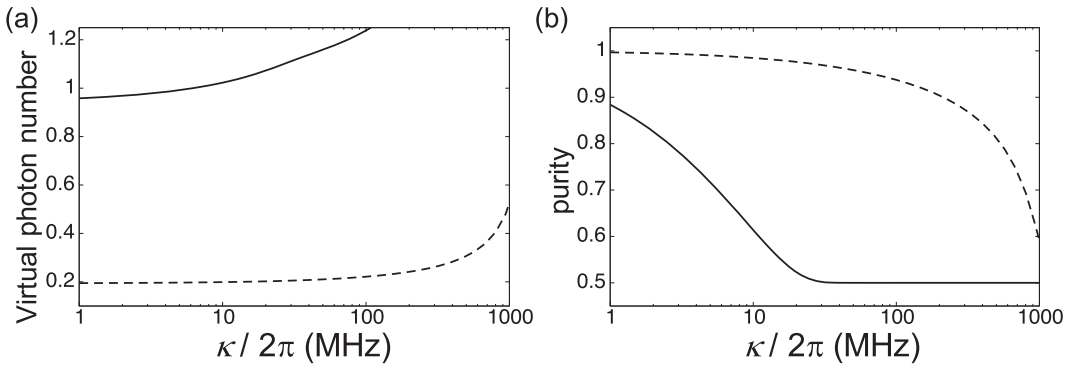

Figure 3. The average number of virtual photons in the resonator (a) and the purity (b) plotted against the bare loss rate κ in the inductive coupling case. The Q–R coupling is $g/2\pi = 3$ GHz (dashed line) and 6 GHz (solid line).

is set to $g/2\pi = 3$ GHz or 6 GHz, which are achievable in circuit QED systems [12, 13]. The other parameters are set to $\omega_r/2\pi = 6$ GHz and $\Delta/2\pi = 1.2$ GHz. See appendix A for the details of parameter settings. We again note that the Q–R coupling is assumed to be inductive in this section, and we refer to the coupling between the resonator and the waveguide when we mention the inductive or capacitive coupling.

4.1. Inductive R–W coupling

We first calculate the average number of virtual photons in the resonator, $\mathrm{tr}[\rho_{\mathrm{ZTS}}a^\dagger a] = |\bar{\alpha}|^2$ in the inductive coupling case. Figure 3(a) shows that, in the inductive coupling case, the number of virtual photons increase as the R–W coupling κ increases. Indeed, the interaction term $\sum_k \xi_k(a + a^\dagger)(b_k + b_k^\dagger)$ acts as a shifter on the resonator phase space in the real direction. Furthermore, we can show that the energy gradient $\partial E/\partial\alpha$ takes a negative value at $\alpha = \tilde{\alpha}$, where $\tilde{\alpha}$ is the stationary solution in the absence of the R–W coupling, which implies that the average number of virtual photons always increases by the R–W coupling, independently of the details of the interaction spectrum ξ_k. In contrast, in reference [26], where the matter is modeled by an ensemble of bosons rather than a qubit, the number of virtual photons decreases by the coupling to the environment. Therefore, whether it increases or decreases depends on the details of the model, e.g. how the matter part is modeled.

Next, we calculate the purity γ of ρ_{ZTS}. Figure 3(b) shows that, in the inductive coupling case, the purity decreases as the loss rate κ increases. By comparing the results for $g/2\pi = 3$ and 6 GHz, we see that the purity also decreases as the Q–R coupling g increases. In other words, in the DSC regime, the quantum coherence of the ground state becomes fragile when the Q–R interaction g is extremely large. It implies that, even though the exact ground state of the quantum Rabi model becomes increasingly useful with increasing g, for instance, for quantum metrological tasks [19], the maximum performance is achieved at a moderate strength of the interaction g when the coupling to the environment is taken into account. Indeed, the nonclassicality, measured by the metrological power [27], has the maximum at a certain value of g, as we discuss below.

Let us evaluate the 'quantumness' of the ground state of the system. There are many ways of defining and quantifying the quantumness [27, 38–41]. Here, we project the state onto the eigenstates of some qubit operator, and calculate the quantumness from the reduced density matrix of the resonator, by exploiting the resource theory of the nonclassicality in continuous variable systems. One of the measures of the nonclassicality is the metrological power [27], which quantifies the maximum achievable quantum enhancement in displacement metrology based on the quantum Fisher information [42, 43]. For a resonator state with the spectral decomposition $\rho_{\mathrm{R}} = \sum_i \lambda_i |i\rangle\langle i|$, the elements of quantum Fisher information matrix for quadrature operators are defined as

$$F_{kl} = 2\sum_{i,j}\frac{(\lambda_i - \lambda_j)^2}{\lambda_i + \lambda_j}\langle i|R^{(k)}|j\rangle\langle j|R^{(l)}|i\rangle, \quad (k,l = 1,2), \tag{15}$$

where $R^{(1)} = (a + a^\dagger)/\sqrt{2}$ and $R^{(2)} = (a - a^\dagger)/\sqrt{2}i$ are the quadrature operators. Then the metrological power of the resonator state ρ_{R} is given by

$$\mathcal{M}(\rho_{\mathrm{R}}) = \max\left\{\frac{\lambda_{\max}(F) - 1}{2}, 0\right\}, \tag{16}$$

where $\lambda_{\max}(F)$ is the maximum eigenvalue of the quantum Fisher information matrix.

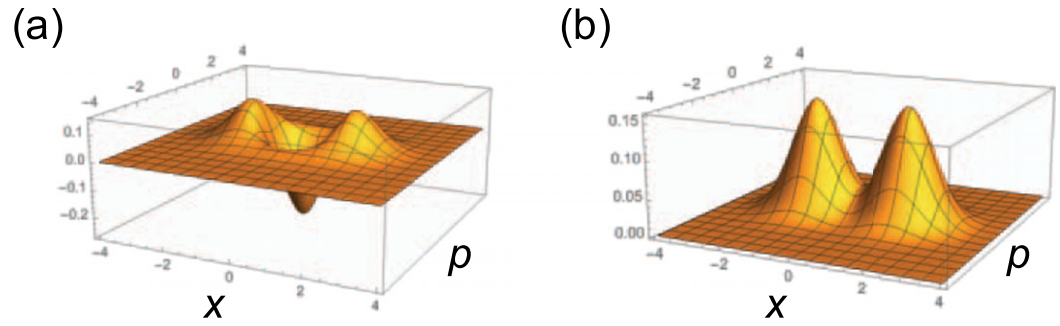

Figure 4. The Wigner functions of the post-measurement state $\rho_{\sigma_x=+1}$ in the inductive coupling case for $g/2\pi = 6$ GHz. (a) $\kappa/2\pi = 1$ MHz. The state possesses sufficient coherence ($C = 0.88$) for the Wigner function to take a negative value around the origin in phase space. (b) $\kappa/2\pi = 40$ MHz. The state is almost decohered ($|C| < 10^{-4}$), and the Wigner function is that of the mixture of two coherent states.

We consider a projective measurement of a qubit operator

$$\sigma_{\theta,\phi} = \sigma_x \sin\theta \cos\phi + \sigma_y \sin\theta \sin\phi + \sigma_z \cos\theta. \tag{17}$$

The measurement outcome $\sigma_{\theta,\phi} = \pm 1$ is obtained with probability

$$\mathrm{Prob}[\sigma_{\theta,\phi} = \pm 1] = \mathrm{tr}\left[P_{\sigma_{\theta,\phi}=\pm 1}\rho_{\mathrm{ZTS}}\right], \tag{18}$$

and the post-measurement state for the resonator is

$$\rho_{\sigma_{\theta,\phi}=\pm 1} \propto \mathrm{tr}_{\mathrm{qubit}}\left[P_{\sigma_{\theta,\phi}=\pm 1}\rho_{\mathrm{ZTS}}\right], \tag{19}$$

where $P_{\sigma_{\theta,\phi}=\pm 1}$ is the projection operator corresponding to the eigenvalue $\sigma_{\theta,\phi} = \pm 1$. Physically, the post-measurement resonator state is a partially decohered cat state possessing interference fringes around the origin in the phase space representation. These fringes become clearer as α and $|C|$ increase, which enables us to measure the displacement more precisely than coherent states (figure 4). We can define the average metrological power as

$$\mathcal{M}^{\mathrm{av}}(\rho_{\mathrm{ZTS}}, \sigma_{\theta,\phi}) = \sum_{a=\pm 1} \mathrm{Prob}[\sigma_{\theta,\phi} = a]\mathcal{M}(\rho_{\sigma_{\theta,\phi}=a}). \tag{20}$$

Finally we define the metrological power of the Q–R system state by optimizing the measurement axis of the qubit as

$$\mathcal{M}(\rho_{\mathrm{ZTS}}) = \max_{\theta,\phi} \mathcal{M}^{\mathrm{av}}(\rho_{\mathrm{ZTS}}, \sigma_{\theta,\phi}). \tag{21}$$

In figure 5, the metrological power of ρ_{ZTS} (equation (21)) is plotted against (a) the loss rate κ and (b) the Q–R coupling g. In our setting, the average metrological power is found to be maximized at $\theta = \phi = \pi/2$, corresponding to the measurement of σ_y. Figure 5(a) shows that for each value of g, the metrological power rapidly decreases to zero when κ becomes larger than a certain value. This critical value of κ becomes small as the Q–R coupling g increases. Figure 5(b) shows that the average metrological power has a maximum at some finite value of g. This maximum is achieved when the loss rate κ is comparable to the energy gap $\Delta e^{-2g^2/\omega_r^2}$, or $g_{\mathrm{opt}} \sim \omega_r\sqrt{\log(\Delta/\kappa)/2}$, so that the optimal coupling strength g_{opt} increases only logarithmically by decreasing κ and increasing Δ. In practice, the loss rate κ cannot be too small because the measurement and control need time duration $T \sim 1/\kappa$, during which decoherence occurs. Therefore, this result implies that it is important to design a circuit to have a proper strength of the Q–R coupling g and the loss rate κ to obtain an optimal metrological advantage.

4.2. Capacitive R–W coupling

The capacitive coupling affects the system much less than the inductive coupling does, as we see below. Indeed, in the capacitive coupling case, the CVS cannot capture the effect of R–W coupling, since it gives the exactly same result as the noninteracting case regardless of the coupling strength, as proved in appendix D. Therefore, we compare the result from the CVS and the numerical diagonalization in the capacitive coupling case, and the CVS in the inductive coupling case. To perform the numerical calculation, the total Hamiltonian is truncated as follows. We take up to 14 photons and 3 photons into account for the resonator mode and each waveguide mode, respectively. As the waveguide modes, we consider four modes with energies $\omega_k/2\pi = 5, 10, 15, 20$ GHz. Although this truncation is not sufficient to quantitatively discuss

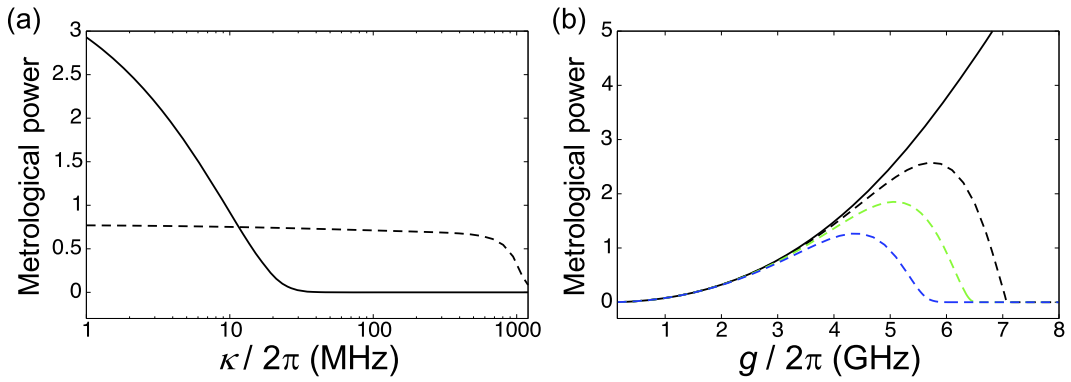

Figure 5. Metrological power $\mathcal{M}$ (equation (21)) plotted against (a) the loss rate κ and (b) the Q–R coupling g in the inductive coupling case. (a) The Q–R coupling is $g/2\pi = 3$ GHz (dashed line) and 6 GHz (solid line). (b) The bare loss rate is $\kappa/2\pi = 0$ (black solid line), 2 MHz (black dashed line), 10 MHz (green dashed line), and 50 MHz (blue dashed line).

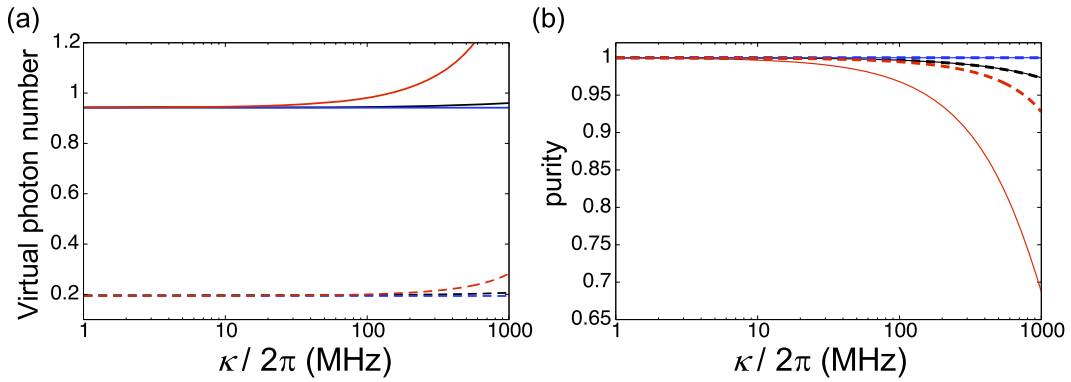

Figure 6. The average number of virtual photons in the resonator (a) and the purity (b) plotted against the bare loss rate κ, calculated from the numerical diagonalization (black) and the CVS (blue) in the capacitive coupling case, and from the CVS in the inductive coupling case (red). The Q–R coupling is $g/2\pi = 3$ GHz (dashed line) and 6 GHz (solid line). The results of the numerical diagonalization for the inductive coupling case are omitted here, and are shown in appendix E.

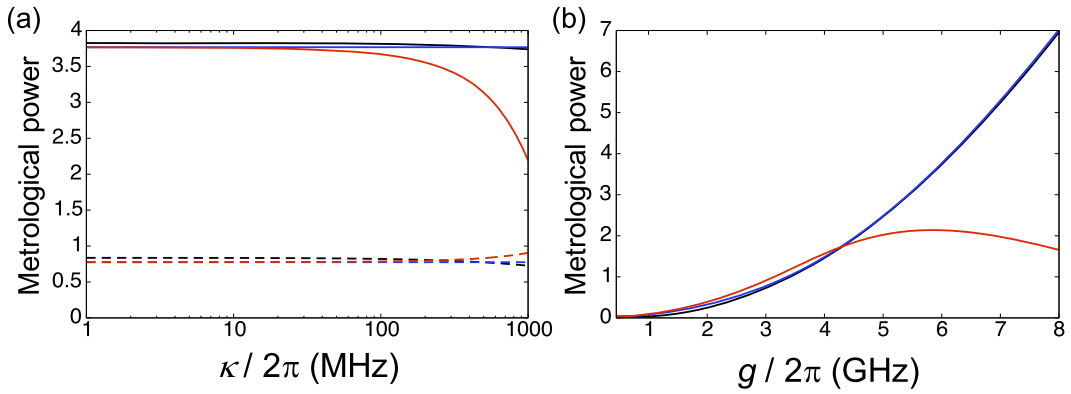

Figure 7. Metrological power $\mathcal{M}$ (equation (21)) plotted against (a) the bare loss rate κ and (b) the Q–R coupling g calculated from the numerical diagonalization (black) and the CVS (blue) in the capacitive coupling case, and from the CVS in the inductive coupling case (red). (a) The Q–R coupling is $g/2\pi = 3$ GHz (dashed line) and 6 GHz (solid line). (b) The loss rate is $\kappa/2\pi = 1000$ MHz.

the effect of the coupling to the environment, the results below clearly show the qualitative difference between the inductive coupling and the capacitive coupling.

In figure 6, the average number of virtual photons (a) and the purity (b) are plotted against the loss rate κ. In the capacitive coupling case, the average number of virtual photons is much less sensitive to the R–W coupling compared to the inductive coupling case. This fact can be qualitatively understood as follows. The coupling operator $X_C = (a - a^\dagger)/i$ acts as a shifter of the displacement α in the imaginary direction.

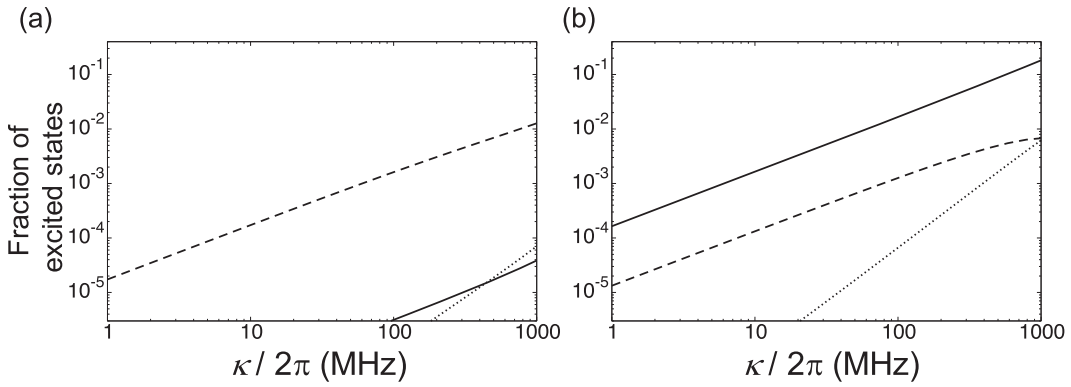

Figure 8. The fraction of the excited states of the isolated system (equation (1)) ($|\phi_0^{(+)}\rangle$ (solid line), $|\phi_1^{(-)}\rangle$ (dashed line) and $|\phi_1^{(+)}\rangle$ (dotted line)) contained in ρ_{ZTS}, calculated from the numerical diagonalization, plotted against the loss rate κ. The R–W coupling is (a) capacitive or (b) inductive.

However, since $\alpha = g/\omega_{\mathrm{r}}$ is real without the environment, the amplitude $|\alpha|^2$ is much less sensitive to the imaginary shift than the real shift. We also see that in figure 6(b), the purity is less affected by the capacitive coupling to the waveguide compared to the inductive coupling case. We will discuss the origin of this stability against the capacitive coupling to the waveguide in section 5.

In figure 7, the average metrological power is plotted against (a) the bare loss rate κ and (b) the Q–R coupling g. Since the effect of the W–R coupling is much underevaluated due to the truncation and the small number of environmental modes, we choose a rather huge value of $\kappa/2\pi = 1000$ MHz, which is formally obtained from equation (9). We see that in the capacitive coupling case, the metrological power calculated from the CVS and the numerical diagonalization agrees very well, and also that the nonclassicality is hardly affected by the capacitive coupling to the waveguide, compared to the inductive coupling case.

5. Stability in the R–W capacitive coupling case

In this section, we discuss the origin of the stability of the ground state when the R–W coupling is capacitive. To obtain some physical insight, let us first consider the case where a bare resonator is coupled to a waveguide. The fraction of the first excited state $|1\rangle$ contained in the total ground state is proportional to $|\langle 1|X|0\rangle|^2$ at the lowest order, where X is a quadrature operator. This transition amplitude is completely insensitive to the type of coupling, i.e. inductive $X_{\mathrm{I}} = a + a^\dagger$ or capacitive $X_{\mathrm{C}} = (a - a^\dagger)/i$, as

$$|\langle 1|X_{\mathrm{I}}|0\rangle|^2 = |\langle 1|X_{\mathrm{C}}|0\rangle|^2 = 1. \tag{22}$$

This is due to the fact that the resonator Hamiltonian $H = \omega_{\mathrm{r}} a^\dagger a$, and the energy eigenstates $|n\rangle$ are invariant under the rotation around the origin in the phase space, represented by the unitary transformation $U = \exp\left(i\theta a^\dagger a\right)$. On the other hand, since the eigenstates of a DSC system are not invariant under this rotation, the transition amplitude strongly depends on the type of coupling as

$$|\langle \phi_0^{(+)}(\alpha)|X_{\mathrm{I}}|\phi_0^{(-)}(\alpha)\rangle|^2 = 4|\mathrm{Re}[\alpha]|^2 = 4\left(\frac{g}{\omega_{\mathrm{r}}}\right)^2, \tag{23}$$

$$|\langle \phi_0^{(+)}(\alpha)|X_{\mathrm{C}}|\phi_0^{(-)}(\alpha)\rangle|^2 = 4|\mathrm{Im}[\alpha]|^2 = 0. \tag{24}$$

Therefore, when the Q–R coupling is mediated by the inductance, i.e. α is real, the system is stable against capacitive coupling to the waveguide. A similar argument is applied in references [44, 45] to protect a qubit from noise based on the fact that the transition amplitude depends on the qubit operator $(\sigma_x, \sigma_y, \sigma_z)$ and can be exponentially small in g. In contrast, in our case, the transition amplitude is exactly zero when the R–W coupling is capacitive.

To see this coupling-type-dependence more directly, we perform a numerical diagonalization of the truncated total Hamiltonian of the Q–R–W system. The truncation is the same as in the previous section. Figure 8 shows the fraction of the excited states of the quantum Rabi model contained in the ground state of H_{tot}. In the inductive coupling case, the most dominant excitation is the first excited state $|\phi_0^{(+)}\rangle$. On the other hand, the fraction of $|\phi_0^{(+)}\rangle$ is not dominant in the capacitive coupling case, as is expected from equation (24). Instead, the most dominant excited state is $|\phi_1^{(-)}\rangle$, which is the only excited state with a nonzero transition amplitude as $|\langle \phi_1^{(-)}(\alpha)|X_{\mathrm{C}}|\phi_0^{(-)}(\alpha)\rangle|^2 = 1$.

Table 1. The transition amplitude between the ground state and the first excited state for several system Hamiltonians and different types of the R–W coupling. Pairs of columns connected by arrows are unitary equivalent.

	inductive R-W coupling		capacitive R-W coupling
bare resonator	$\lvert\langle 1\rvert X_I\rvert 0\rangle\rvert^2 = 1$	$\Leftrightarrow$	$\lvert\langle 1\rvert X_C\rvert 0\rangle\rvert^2 = 1$
qubit+resonator (inductive)	$\lvert\langle \phi_0^{(+)}\rvert X_I\rvert \phi_0^{(-)}\rangle\rvert^2 = 4(g/\omega_{\rm r})^2$	$\nLeftrightarrow$	$\lvert\langle \phi_0^{(+)}\rvert X_C\rvert \phi_0^{(-)}\rangle\rvert^2 = 0$
qubit+resonator (capacitive)	$\lvert\langle \phi_0^{(+)}\rvert X_I\rvert \phi_0^{(-)}\rangle\rvert^2 = 0$	$\nLeftrightarrow$	$\lvert\langle \phi_0^{(+)}\rvert X_C\rvert \phi_0^{(-)}\rangle\rvert^2 = 4(g/\omega_{\rm r})^2$

The reason why the system is not changed in the capacitive coupling case in the CVS analysis in section 4 is that the CVS considers only the two lowest eigenstates $|\phi_0^{(-)}\rangle$ and $|\phi_0^{(+)}\rangle$. From the analysis performed in section 4, we cannot determine whether the metrological power monotonically increases as a function of g or peaks at a certain value of g in the capacitive coupling case. However, the peak, if it exists, is expected to occur at a much larger value of g than in the inductive coupling case, so that a higher metrological power is achievable in the capacitive coupling case.

We need to be careful to conclude from our results that the capacitive R–W coupling is superior to the inductive coupling, since there is a tradeoff between the gate speed and the relaxation time [46]. In the capacitive coupling case, this tradeoff relation indicates that the long relaxation time implies a slow control between the ground state and the first excited state.

Finally, we stress that only the relative phase between the resonator quadrature operators coupled to the qubit and the waveguide is relevant to this stability. When the Q–R coupling is assumed to be capacitive, the system is sensitive to the capacitive R–W coupling and insensitive to the inductive R–W coupling. These results are summarized in table 1.

6. Conclusion

In this paper, by analyzing the ground state of a Q–R–W system, we have investigated the effect of an environment on the ground state of the quantum Rabi model in the DSC regime. We have introduced the qubit-state-dependent CVS (equation (10)). This variational ansatz is easy to analyze and is consistent with the results from numerical diagonalization and perturbation theory. We have shown that the zero-temperature state $\rho_{\rm ZTS}$ strongly depends on the type of the R–W coupling because of the broken rotational symmetry in the eigenstates of the DSC system.

When the resonator couples to the qubit and the waveguide in the same way (for instance, both are inductive), the number of virtual photons increases due to the R–W coupling, which might be advantageous to detect virtual photons experimentally [47, 48]. We have also shown that, even at zero temperature, the Q–R system is in a mixed state and contains the excited states of the quantum Rabi Hamiltonian, which implies the fragility of the quantum superposition realized in the ground state. As a result, the nonclassicality of the resonator system, measured by the metrological power, is maximized at a certain coupling strength g, when the environment is taken into account. We note that the analysis based on the multi-polaron expansion [49] suggests that the CVS underestimate the coherence in the system. To obtain a more accurate result in the inductive coupling case, we may modify the CVS to include more than one polaron.

On the other hand, when the resonator couples to the qubit and the waveguide in different ways (for instance, one is inductive and the other is capacitive), the system is almost unaffected, so that a higher metrological power than the same coupling case is achievable in the presence of environment. It is worth considering a better variational ansatz that can quantitatively describe the ground state in such case.

Our results offer guiding principles to obtain a better metrological advantage when we design superconducting circuit QED systems. Since it is necessary to perform projective measurements on the qubit to exploit this metrological advantage, our results also demonstrate the advantages of achieving dynamically controllable coupling between qubit and resonator.

Acknowledgments

We would like to thank S Masuda, R Takagi, and I Iakoupov for fruitful discussions. This work was supported by Japan Science and Technology Agency (JST) Core Research for Evolutionary Science and

Technology (Grant No. JPMJCR1775), JST Precursory Research for Embryonic Science and Technology (Grant No. JPMJPR1767), and Japan Society for the Promotion of Science KAKENHI (Grant No. 19K03684).

Data availability statement

The data that support the findings of this study are available upon reasonable request from the authors.

Appendix A. Derivation of the Hamiltonian of the circuit coupled to two waveguides

In this section, we derive the Hamiltonians of the circuits in figures 2(a) and (b). For that purpose, we consider a Q–R circuit coupled to two waveguides, one inductively and one capacitively, as shown in figure A1. The circuits in figures 2(a) and (b) can be obtained by taking the limits $L_c \to \infty$ and $C_c \to 0$, respectively. We note that a similar circuit is discussed in reference [50].

We assign a flux variable to each vertex. Here, variables ψ, ϕ, Φ_j and Ψ_j represent degrees of freedom of the qubit, the resonator, the waveguide coupled inductively (left), and the waveguide coupled capacitively (right), respectively. The shaded area in figure A1 can be an arbitrary circuit constituting a qubit, such as a Cooper pair box or a flux qubit. We do not specify the details of the qubit circuit, but assume that it involves only ψ and $\dot{\psi}$. Then the total Lagrangian is given by

$$\begin{aligned}\mathcal{L}(\psi,\phi,\Phi_j,\Psi_j,\dot{\psi},\dot{\phi},\dot{\Phi}_j,\dot{\Psi}_j)&\\ &= \mathcal{L}_{\rm M}(\psi,\dot{\psi}) - \frac{(\phi-\psi)^2}{2L_{\rm R}} + \frac{C_{\rm R}\dot{\phi}^2}{2}\\ &\quad - \frac{(\phi-\Phi_0)^2}{2L_{\rm c}} + \sum_{j=0}^{\infty}\left(\frac{C_{\rm T}\Delta x\dot{\Phi}_j^2}{2} - \frac{(\Phi_{j+1}-\Phi_j)^2}{2L_{\rm T}\Delta x}\right)\\ &\quad + \frac{C_{\rm c}}{2}(\dot{\phi}-\dot{\Psi}_0)^2 + \sum_{j=0}^{\infty}\left(\frac{C_{\rm T}\Delta x\dot{\Psi}_j^2}{2} - \frac{(\Psi_{j+1}-\Psi_j)^2}{2L_{\rm T}\Delta x}\right).\end{aligned} \tag{A.1}$$

Canonical conjugate variables are defined as

$$q = \frac{\partial\mathcal{L}}{\partial\dot{\phi}} = C_{\rm R}\dot{\phi} + C_{\rm c}(\dot{\phi}-\dot{\Psi}_0), \tag{A.2}$$

$$\bar{q} = \frac{\partial\mathcal{L}}{\partial\dot{\psi}} = \frac{\partial\mathcal{L}_{\rm M}}{\partial\dot{\psi}}, \tag{A.3}$$

$$Q_j = \frac{\partial\mathcal{L}}{\partial\dot{\Phi}_j} = C_{\rm T}\Delta x\dot{\Phi}_j \ (j\geq 0), \tag{A.4}$$

$$\bar{Q}_0 = \frac{\partial\mathcal{L}}{\partial\dot{\Psi}_0} = C_{\rm c}(\dot{\Psi}_0-\dot{\phi}), \tag{A.5}$$

$$\bar{Q}_j = \frac{\partial\mathcal{L}}{\partial\dot{\Psi}_j} = C_{\rm T}\Delta x\dot{\Psi}_j \ (j\geqslant 1). \tag{A.6}$$

By performing the Legendre transformation, we obtain the Hamiltonian of the total circuit as

$$\begin{aligned}H &= \left(\bar{q}\dot{\psi} - \mathcal{L}_{\rm M} - \frac{\phi\psi}{L_{\rm R}} + \frac{\psi^2}{2L_{\rm R}}\right) + \left(\frac{q^2}{2C_{\rm R}} + \frac{\phi^2}{2L_{\rm R}}\right)\\ &\quad + \left[\frac{\Phi_0^2}{2L_{\rm C}} + \sum_{j=0}^{\infty}\left(\frac{Q_j^2}{2C_{\rm T}\Delta x} + \frac{(\Phi_{j+1}-\Phi_j)^2}{2L_{\rm T}\Delta x}\right)\right]\\ &\quad + \left[\frac{\bar{Q}_0^2}{2C_{\rm c}} + \sum_{j=0}^{\infty}\left(\frac{\bar{Q}_j^2}{2C_{\rm T}\Delta x} + \frac{(\Psi_{j+1}-\Psi_j)^2}{2L_{\rm T}\Delta x}\right)\right] - \frac{\phi\Phi_0}{L_{\rm c}} + \frac{q\bar{Q}_0}{C_{\rm R}},\end{aligned} \tag{A.7}$$

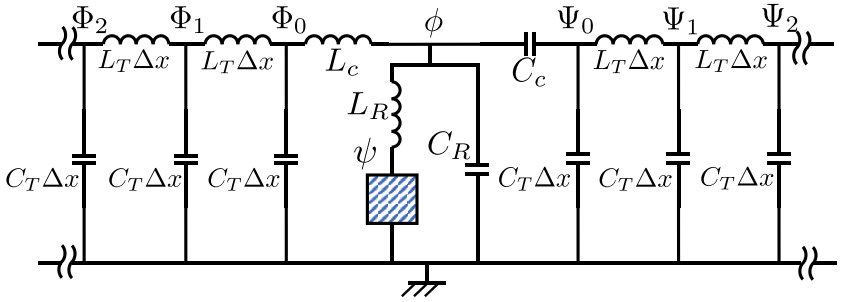

Figure A1. Circuit diagram of the Q–R system coupled to two waveguides, one inductively (left) and one capacitively (right).

where $L'_{\rm R} = \frac{L_{\rm c}L_{\rm R}}{L_{\rm c}+L_{\rm R}}$ and $C'_{\rm c} = \frac{C_{\rm c}C_{\rm R}}{C_{\rm c}+C_{\rm R}}$. The first line represents the Hamiltonian for the qubit, the resonator, and the interaction between them. The second (third) line represents the Hamiltonian for the waveguide inductively (capacitively) coupled to the resonator. The final line represents the interaction between the resonator and the waveguide modes. We note that the qubit variables $\{\psi, \bar{q}\}$ do not appear except for the first term line. To diagonalize the waveguide modes, let us consider the equations of motion for the waveguide variables:

$$\dot{Q}_j = \frac{\Phi_{j+1} + \Phi_{j-1} - 2\Phi_j}{L_{\rm T}\Delta x} \ (j \geqslant 1), \tag{A.8}$$

$$\dot{\Phi}_j = \frac{Q_j}{C_{\rm T}\Delta x} \ (j \geqslant 1), \tag{A.9}$$

$$\dot{Q}_0 = -\frac{\Phi_0}{L_{\rm c}} - \frac{\Phi_0 - \Phi_1}{L_{\rm T}\Delta x}, \tag{A.10}$$

$$\dot{\Phi}_0 = \frac{Q_0}{C_{\rm T}\Delta x}, \tag{A.11}$$

$$\dot{\bar{Q}}_j = \frac{\Psi_{j+1} + \Psi_{j-1} - 2\Psi_j}{L_{\rm T}\Delta x} \ (j \geqslant 1), \tag{A.12}$$

$$\dot{\Psi}_j = \frac{\bar{Q}_j}{C_{\rm T}\Delta x} \ (j \geqslant 1), \tag{A.13}$$

$$\dot{\bar{Q}}_0 = -\frac{\Psi_0 - \Psi_1}{L_{\rm T}\Delta x}, \tag{A.14}$$

$$\dot{\Psi}_0 = \frac{\bar{Q}_0}{C'_{\rm c}}. \tag{A.15}$$

From these equations, by taking the continuous limit, $\Delta x \to 0$, $\Phi_j \to \Phi(x) = \Phi(j\Delta x)$, and $\Psi_j \to \Psi(x) = \Psi(j\Delta x)$, we obtain the wave equations for $x > 0$ as

$$\ddot{\Phi}(x) = \frac{1}{C_{\rm T}L_{\rm T}}\frac{\partial^2\Phi(x)}{\partial x^2}, \tag{A.16}$$

$$\ddot{\Psi}(x) = \frac{1}{C_{\rm T}L_{\rm T}}\frac{\partial^2\Phi(x)}{\partial x^2}, \tag{A.17}$$

with boundary conditions

$$0 = -\frac{\Phi(+0)}{L_{\rm c}} + \frac{1}{L_{\rm T}}\frac{\partial\Phi(x)}{\partial x}\bigg|_{x=+0}, \tag{A.18}$$

$$\ddot{\Psi}(+0) = \frac{1}{C'_{\rm c}L_{\rm T}}\frac{\partial\Psi(x)}{\partial x}\bigg|_{x=+0}. \tag{A.19}$$

Let us consider the inductively-coupled waveguide modes. The eigenfunction with frequency ω is given by

$$f_\omega(x) = \sqrt{\frac{2}{L}}\frac{\cos\left(\frac{\omega}{v}x\right) + \zeta_{\rm I}(\omega)\sin\left(\frac{\omega}{v}x\right)}{\sqrt{1+\zeta_{\rm I}(\omega)^2}}, \tag{A.20}$$

where L is the length of the waveguide, $v = 1/\sqrt{L_T C_T}$ is the speed of microwaves in the waveguide, and $\zeta(\omega) = L_T v/L_C\omega$ is a dimensionless quantity defining the phase of the eigenfunction. Then the positive frequency part of the flux variable $\Phi(x)$ is quantized as

$$\Phi(x)^+ = \sum_k \sqrt{\frac{\hbar Z_T v}{2\omega_k}} f_{\omega_k}(x) b_k, \tag{A.21}$$

where $Z_T = \sqrt{L_T/C_T}$ is the characteristic impedance, b_k is the annihilation operator of the eigenmode $f_{\omega_k}(x)$, and $\omega_k = \pi k v/L$. Therefore, the flux variables Φ_0 and ϕ are expressed in terms of the creation and annihilation operators as

$$\Phi_0 = \sum_k \frac{\hbar Z_T v}{\omega_k L} \frac{b_k + b_k^\dagger}{\sqrt{1+\zeta(\omega_k)^2}} \to \int_0^\infty d\omega \sqrt{\frac{\hbar Z_T}{\pi\omega}} \frac{b(\omega) + b(\omega)^\dagger}{\sqrt{1+\zeta(\omega)^2}}, \tag{A.22}$$

$$\phi = \sqrt{\frac{\hbar Z_R}{2}}(a + a^\dagger), \tag{A.23}$$

where the limit $L \to \infty$ is taken in the second line. Here, $a(a^\dagger)$ is the annihilation (creation) operator of microwave photons in the resonator. The characteristic impedance for the resonator Z_R is defined as $Z_R = \sqrt{L_R'/C_R}$. By substituting equations (A.22) and (A.23) to the inductive coupling term $-\phi\Phi_0/L_c$, we obtain

$$-\frac{\phi\Phi_0}{L_c} = -\int_0^\infty d\omega\, \xi_0^I \sqrt{\frac{\omega}{1+(\omega/\omega_{cutoff}^I)^2}}(a + a^\dagger)(b(\omega) + b(\omega)^\dagger), \tag{A.24}$$

where

$$\xi_0^I = \hbar\sqrt{\frac{1}{2\pi}\cdot\frac{Z_R}{Z_T}}, \tag{A.25}$$

$$\omega_{cutoff}^I = \frac{Z_T}{L_c}. \tag{A.26}$$

In a similar manner, we obtain the capacitive coupling term as

$$\frac{q\bar{Q}_0}{C_R} = \int_0^\infty d\omega\, \xi_0^C \sqrt{\frac{\omega}{1+(\omega/\omega_{cutoff}^C)^2}}(a - a^\dagger)(d(\omega) - d(\omega)^\dagger), \tag{A.27}$$

where

$$\xi_0^C = \hbar\sqrt{\frac{1}{2\pi}\cdot\frac{Z_T C_c'^2}{Z_R C_R^2}}, \tag{A.28}$$

$$\omega_{cutoff}^C = \frac{1}{Z_T C_c'}, \tag{A.29}$$

and $d(\omega)$ is the annihilation operator of the capacitively-coupled waveguide mode with frequency ω.

We note that the interaction spectrums ξ_k^I and ξ_k^C satisfy the inequality

$$\sum_k \frac{\xi_k^{X\,2}}{\omega_k} < \frac{\omega_r}{4} \quad (X = I, C), \tag{A.30}$$

which ensures that there is no bosonic mode with negative energy. In this sense, the circuit used in our analysis shows no superradiance-like instability.

In the numerical calculation, the parameters are set to be $\omega_r/2\pi = 6$ GHz, $\Delta/2\pi = 1.2$ GHz, $Z_W = 50\ \Omega$, and $Z_R = 30\ \Omega$. In figure A2, the values of κ and ω_{cutoff} are plotted as a function of the coupling inductance or capacitance in each case. Since the left waveguide is directly connected to the Q–R system through the coupling inductance L_c, κ^I takes a large value unless L_c is sufficiently large, and is a decreasing function of L_c. This property is special to the circuit in figure A1, and different from the circuits realized in references [12, 13], where the waveguide is coupled to the resonator through mutual inductance.

Appendix B. Relation to the spin-boson model

In this section, we show that the Hamiltonian describing the circuit in figure 2(b) can be effectively mapped to the spin-boson model [35]. We note that the mapping can be exactly performed if we first diagonalize the

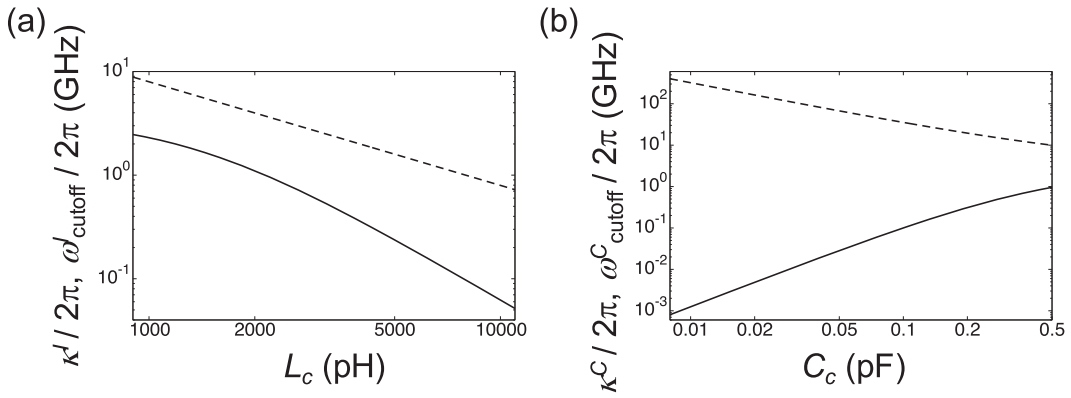

Figure A2. Values of κ (solid line) and $\omega_{\rm cutoff}$ (dashed line) plotted against (a) the coupling inductance (L_c) and (b) the coupling capacitance (C_c).

bosonic (R–W) part and consider it as the environment [37, 51]. The difficulty of this approach seems that it is difficult to obtain the information on the reduced density matrix of the Q–R system. Instead, we chose a different approach where we first (approximately) diagonalize the Q–R system and then consider the interaction with the waveguide, by which we can easily discuss the state of the Q–R system.

The total Hamiltonian is given by

$$H_{\rm tot} = H_{\rm S} + H_{\rm E} + H_{\rm SE}, \tag{B.1}$$

where

$$H_{\rm S} = \omega_{\rm r} a^\dagger a + \frac{\Delta}{2}\sigma_x + g\sigma_z(a + a^\dagger), \tag{B.2}$$

$$H_{\rm SE} = \sum_k \xi_k (a + a^\dagger)(b_k + b_k^\dagger), \tag{B.3}$$

$$H_{\rm E} = \sum_k \omega_k b_k^\dagger b_k. \tag{B.4}$$

To map the total Hamiltonian to the spin-boson model, we project the state space of the Q–R system onto the space spanned by the two low-lying energy states, $\{|\phi_0^{(-)}(\alpha)\rangle, |\phi_0^{(+)}(\alpha)\rangle\}$. Let $\bar{\sigma}_j$ $(j = x, y, z)$ be the Pauli matrix in the basis of $\{|\uparrow\rangle\,|-\alpha\rangle, |\downarrow\rangle\,|\alpha\rangle\}$. Then the truncated Hamiltonian becomes the spin-boson model,

$$\frac{\Delta e^{-2\alpha^2}}{2}\bar{\sigma}_x + \sum_k \xi_k \bar{\sigma}_z (b_k + b_k^\dagger) + \sum_k \omega_k b_k^\dagger b_k. \tag{B.5}$$

Here, the 'localized state' corresponds to $|\uparrow\rangle\,|-\alpha\rangle$ and $|\downarrow\rangle\,|\alpha\rangle$.

The spectral function of this truncated Hamiltonian can be calculate as

$$\begin{aligned} J(\omega) &= \frac{\pi}{2}\sum_k 32\,{\rm Re}[\alpha]^2 \xi_k^2 \delta(\omega - \omega_k) \\ &= 16\pi\,{\rm Re}[\alpha]^2 \xi_0^2 \omega \frac{1}{1 + (\omega/\omega_{\rm cutoff})^2}, \end{aligned} \tag{B.6}$$

which corresponds to the Ohmic case.

Appendix C. Symmetry of the total Hamiltonian and the CVS

The total Hamiltonian is invariant under a parity transformation $a \leftrightarrow -a$, $b_k \leftrightarrow -b_k$, and $|\uparrow\rangle \leftrightarrow |\downarrow\rangle$. The ground state is expected to have the same symmetry, so that

$$\begin{aligned} &c_0\,|\uparrow\rangle \otimes |\alpha; \{\beta_j\}\rangle + c_1\,|\downarrow\rangle \otimes |\alpha'; \{\beta_j'\}\rangle \\ &\quad = e^{i\theta}(c_0\,|\downarrow\rangle \otimes |-\alpha; \{-\beta_j\}\rangle + c_1\,|\uparrow\rangle \otimes |-\alpha'; \{-\beta_j'\}\rangle). \end{aligned} \tag{C.1}$$

Then we have

$$\alpha = -\alpha', \tag{C.2}$$

$$\beta_j = -\beta'_j, \tag{C.3}$$

$$c_0 = e^{i\theta} c_1, \tag{C.4}$$

$$c_1 = e^{i\theta} c_0. \tag{C.5}$$

From the last two equations, we have $e^{i\theta} = \pm 1$ and $|c_0| = |c_1| = 1/\sqrt{2}$ from the normalization condition. The choice of sign only affects the qubit energy term $\Delta\sigma_x$, and $e^{i\theta} = -1$ is chosen so that the qubit energy term reduces the total energy.

Appendix D. Stationary state equations for CVS

In this section, we derive the stationary state equations that the variational parameters of CVS should satisfy to minimize the total energy. The total energy of the CVS is

$$\begin{aligned} E_{\mathrm{CVS}} &= \langle \psi_{\mathrm{C}}(\alpha, \{\beta_k\}) | H_{\mathrm{tot}} | \psi_{\mathrm{C}}(\alpha, \{\beta_k\}) \rangle \\ &= \omega_{\mathrm{r}} |\alpha|^2 - g(\alpha + \alpha^*) + \sum_k \omega_k |\beta_k|^2 \\ &\quad \pm \sum_k \xi_k (\alpha \pm \alpha^*)(\beta_k \pm \beta_k^*) - \frac{\Delta}{2} \exp\left[-2 \left(|\alpha|^2 + \sum_k |\beta_k|^2 \right) \right], \end{aligned} \tag{D.1}$$

depending on whether the R–W coupling is inductive or capacitive. The variational parameters minimizing the total energy should satisfy $\partial E_{\mathrm{CVS}}/\partial \alpha^* = 0$ and $\partial E_{\mathrm{CVS}}/\partial \beta_k^* = 0, \forall k$, which read

$$\omega_{\mathrm{r}} \alpha + \Delta \alpha \exp\left[-2 \left(|\alpha|^2 + \sum_k |\beta_k|^2 \right) \right] - g + \sum_k \xi_k (\beta_k \pm \beta_k^*) = 0, \tag{D.2}$$

$$\omega_k \beta_k + \Delta \beta_k \exp\left[-2 \left(|\alpha|^2 + \sum_k |\beta_k|^2 \right) \right] + \xi_k (\alpha \pm \alpha^*) = 0, \forall k. \tag{D.3}$$

From equation (D.3), β_k can be expressed in terms of α and the collective variable $S = \sum_k \beta_k^* \beta_k$ as follows:

$$\beta_k = -\frac{\xi_k (\alpha \pm \alpha^*)}{\omega_k + \Delta e^{-2(\alpha^* \alpha + S)}}. \tag{D.4}$$

In the inductive coupling case, we have

$$\beta_k = -\frac{2\xi_k \mathrm{Re}[\alpha]}{\omega_k + \Delta e^{-2(\alpha^* \alpha + S)}}, \tag{D.5}$$

which is real. Substituting equation (D.5) into equation (D.2) and the definition of S, we obtain

$$\omega_{\mathrm{r}} \alpha + \Delta \alpha e^{-2(\alpha^* \alpha + S)} - g - 4\,\mathrm{Re}[\alpha] f_1(\Delta e^{-2(\alpha^* \alpha + S)}) = 0, \tag{D.6}$$

$$4\,\mathrm{Re}[\alpha]^2 f_2(\Delta e^{-2(\alpha^* \alpha + S)}) = S, \tag{D.7}$$

where we have defined

$$f_1(x) = \sum_k \frac{\xi_k^2}{x + \omega_k}, \tag{D.8}$$

$$f_2(x) = \sum_k \frac{\xi_k^2}{(x + \omega_k)^2}. \tag{D.9}$$

From equation (D.6), we see that α is also real. Although there are originally an infinitely large number of parameters $\{\beta_k\}$, we obtain a set of closed equations for α and S, and once we obtain the stationary solution for $\bar{\alpha}$ and $\bar{S}$, β_k can be obtained from equation (D.5). In the continuous limit of $L \to \infty$, $f_1(x)$ and $f_2(x)$ can be explicitly calculated as follows:

$$f_1(x) \to \frac{\xi_0^2 \omega_{\mathrm{cutoff}}^2}{x^2 + \omega_{\mathrm{cutoff}}^2} \left(-x \log \frac{\omega_{\mathrm{cutoff}}}{x} + \frac{\pi \omega_{\mathrm{cutoff}}}{2} \right), \tag{D.10}$$

$$f_2(x) \to \xi_0^2 \omega_{\mathrm{cutoff}}^2 \left(-\frac{1}{x^2 + \omega_{\mathrm{cutoff}}^2} + \frac{x^2 - \omega_{\mathrm{cutoff}}^2}{(x^2 + \omega_{\mathrm{cutoff}}^2)^2} \log \frac{x}{\omega_{\mathrm{cutoff}}} + \frac{\pi \omega_{\mathrm{cutoff}} x}{(x^2 + \omega_{\mathrm{cutoff}}^2)^2} \right). \tag{D.11}$$

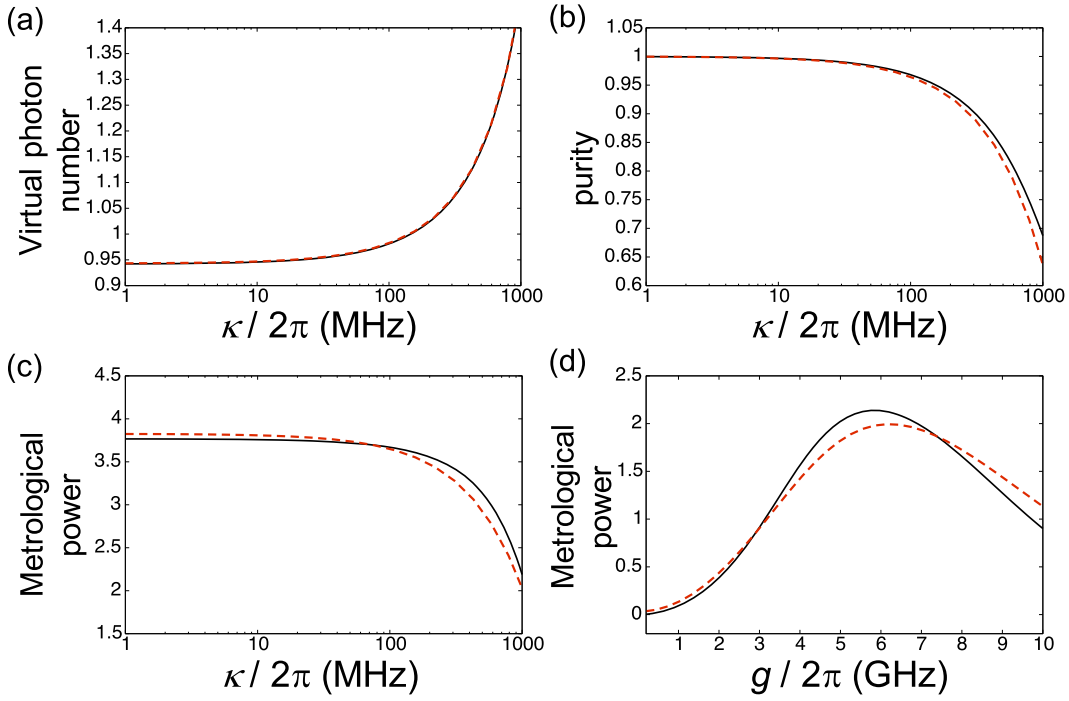

Figure E1. The average number of virtual photons in the resonator (a), the purity (b), and the average metrological power, plotted against the bare loss rate κ. (d) The average metrological power plotted against the Q–R coupling strength g. All the quantities are calculated from the CVS (black solid line) and the numerical diagonalization (red dashed line). The loss rate is set to $\kappa/2\pi = 1000$ MHz, and the Q–R coupling is set to $g/2\pi = 6$ GHz.

In the capacitive coupling case, we have

$$\beta_k = -\frac{2i\xi_k \,\mathrm{Im}[\alpha]}{\omega_k + \Delta e^{-2(\alpha^*\alpha+S)}}, \tag{D.12}$$

which is purely imaginary. Substituting equation (D.5) into equation (D.2), we obtain

$$\omega_r\alpha + \Delta\alpha e^{-2(\alpha^*\alpha+S)} - g + i\sum_k 4\,\mathrm{Im}[\alpha] f_1(\Delta e^{-2(\alpha^*\alpha+S)}) = 0. \tag{D.13}$$

Subtracting equation (D.13) from its complex conjugate, we obtain

$$(\omega_k + \Delta e^{-2(\alpha^*\alpha+S)})(\alpha - \alpha^*) = 0, \tag{D.14}$$

so that α is real. Since $\mathrm{Im}[\alpha] = 0$, we have $\beta_k = 0$ from equation (D.12) and hence $S = 0$, and finally we obtain a closed equation for α as

$$(\omega_r + \Delta e^{-2\alpha^2})\alpha = g. \tag{D.15}$$

Equation (D.15) is the same as the stationary state equation for the closed quantum Rabi model, i.e. $\xi_k = 0$. This result means that the CVS does not provide a good approximation for the Q–R–W ground state in this case.

Appendix E. Validity of CVS in inductive coupling

In this appendix, we confirm the validity of the CVS in the inductive coupling case. First, we compare the result from the CVS and the numerical diagonalization for a few waveguide mode case. We see that in figures E1(a) and (b), the number of virtual photons and the purity calculated from the CVS and the numerical diagonalization agree quantitatively. We also see that from figures E1(c) and (d), the nonclassical property of the system, measured by the metrological power can also be described by the CVS.

Next, we compare the result from the CVS and perturbation theory. At the leading order in ξ_k, ρ_{ZTS} is given by

$$\begin{aligned}\rho_{\mathrm{ZTS}} = {} & (1 - 4\alpha^2 f_2(\Delta e^{-2\alpha^2}) - f_2(2\alpha^2\Delta e^{-2\alpha^2} + \omega_r))|\psi_0^{(-)}(\alpha)\rangle\langle\psi_0^{(-)}(\alpha)| \\ & + 4\alpha^2 f_2(\Delta e^{-2\alpha^2})|\psi_0^{(+)}(\alpha)\rangle\langle\psi_0^{(+)}(\alpha)| + f_2(2\alpha^2\Delta e^{-2\alpha^2} + \omega_r)|\psi_1^{(-)}(\alpha)\rangle\langle\psi_1^{(-)}(\alpha)| + o(\xi_k^2),\end{aligned} \tag{E.1}$$

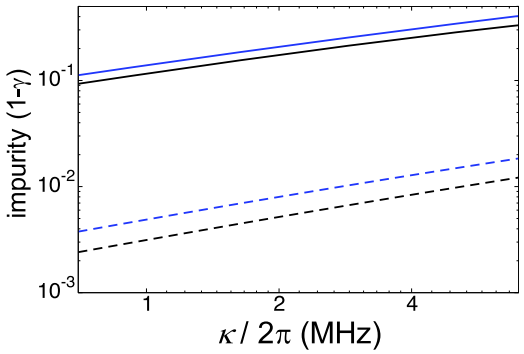

Figure E2. The impurity ($=1-\gamma$) plotted against the bare loss rate κ, calculated from the CVS (black) and perturbation theory (blue). The Q–R coupling is set to $g/2\pi = 3$ GHz (dashed line) and 6 GHz (solid line). All the quantities are calculated from the CVS (black solid line) and the numerical diagonalization (red dashed line).

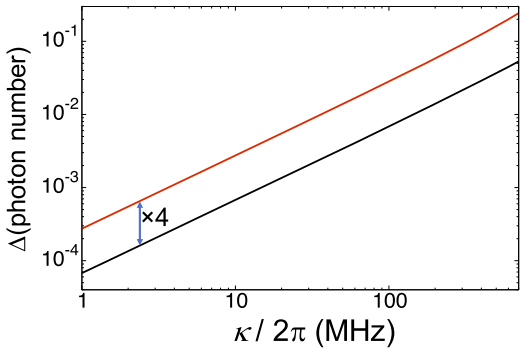

Figure F1. Increase of virtual photons from the noninteracting ($\xi_k = 0$) case, plotted against the bare loss rate κ. The black (red) line shows the result from the numerical diagonalization with (without) the RWA in the R–W coupling. The Q–R coupling is set to $g/2\pi = 6$ GHz.

where $\alpha = g/\omega_r$. Figure E2 shows that the impurity $(1-\gamma)$ calculated from the CVS and perturbation theory have the same scaling to κ and are in good agreement. The small deviation is attributed to the fact that the qubit energy Δ is finite, and equation (3) is no longer exact. Note that equation (3) remains a good approximation for the eigenstates of the quantum Rabi model when $\omega_r \gg \Delta$ or $g \gg \omega_r, \Delta$.

Appendix F. Effect of counter-rotating terms in R–W coupling

In this section, we discuss the effect of counter-rotating terms and the RWA in the R–W coupling. In quantum mechanical analysis, the co-rotating and counter-rotating terms describe transitions to virtual intermediate states. If the virtual state is far off resonance, its effect is suppressed. Since the counter-rotating terms typically involve the virtual states far off resonant, they give smaller contributions than the co-rotating terms, which justify the RWA.

In contrast, since the CVS is a semiclassical approach, where the annihilation operators a and b_k are replaced with the c-numbers, α and β_k, respectively, there is no similar distinction between the co-rotating and counter-rotating terms. Indeed, in the inductive coupling case, noting that α and β_k are real quantities, the co-rotating terms $(ab_k^\dagger + a^\dagger b_k)$ and the counter-rotating terms $(ab_k + a^\dagger b_k^\dagger)$ give the same contribution to the CVS energy functional in equation (11). Then, performing the RWA is equivalent to changing the coupling constant $\xi_k \to \xi_k/2$ in the CVS analysis. Therefore, the number of virtual photons increases even if we perform the RWA. Furthermore, the increase in virtual photons with RWA is $\sim$4 times smaller than without RWA, since the increase of virtual photons is $O(\xi_k^2)$ at the lowest-order perturbation. This simple analysis based on the CVS is in good agreement with the result from the numerical diagonalization as shown in figure F1, which justifies the symmetric treatment of the co-rotating terms and the counter-rotating terms in the DSC regime.

ORCID iDs

Tomohiro Shitara https://orcid.org/0000-0002-1799-9100
Motoaki Bamba https://orcid.org/0000-0001-9811-0416
Sahel Ashhab https://orcid.org/0000-0003-1931-1178
Kazuki Koshino https://orcid.org/0000-0002-9754-4463

References

[1] Rabi I I 1937 Space quantization in a gyrating magnetic field *Phys. Rev.* **51** 652
[2] Jaynes E T and Cummings F W 1963 Comparison of quantum and semiclassical radiation theories with application to the beam maser *Proc. IEEE* **51** 89
[3] Walls D F and Milburn G J 2008 *Quantum Optics* (Berlin: Springer)
[4] Gleyzes S, Kuhr S, Guerlin C, Bernu J, Deléglise S, Busk Hoff U, Brune M, Raimond J-M and Haroche S 2007 Quantum jumps of light recording the birth and death of a photon in a cavity *Nature* **446** 297
[5] Göppl M *et al* 2008 Coplanar waveguide resonators for circuit quantum electrodynamics *J. Appl. Phys.* **104** 113904
[6] Blais A, Huang R S, Wallraff A, Girvin S M and Schoelkopf R J 2004 Cavity quantum electrodynamics for superconducting electrical circuits: an architecture for quantum computation *Phys. Rev.* A **69** 062320
[7] Blais A, Gambetta J, Wallraff A, Schuster D I, Girvin S M, Devoret M H and Schoelkopf R J 2007 Quantum-information processing with circuit quantum electrodynamics *Phys. Rev.* A **75** 032329
[8] Billangeon P M, Tsai J S and Nakamura Y 2015 Scalable architecture for quantum information processing with superconducting flux qubits based on purely longitudinal interactions *Phys. Rev.* B **92** 020509(R)
[9] Billangeon P M, Tsai J S and Nakamura Y 2015 Circuit-QED-based scalable architectures for quantum information processing with superconducting qubits *Phys. Rev.* B **91** 094517
[10] Forn-Díaz P, García-Ripoll J J, Peropadre B, Orgiazzi J-L, Yurtalan M A, Belyansky R, Wilson C M and Lupascu A 2017 Ultrastrong coupling of a single artificial atom to an electromagnetic continuum in the nonperturbative regime *Nat. Phys.* **13** 39
[11] Yoshihara F, Fuse T, Ashhab S, Kakuyanagi K, Saito S and Semba K 2017 Characteristic spectra of circuit quantum electrodynamics systems from the ultrastrong- to the deep-strong-coupling regime *Phys. Rev.* A **95** 053824
[12] Yoshihara F, Fuse T, Ashhab S, Kakuyanagi K, Saito S and Semba K 2017 Superconducting qubit–oscillator circuit beyond the ultrastrong-coupling regime *Nat. Phys.* **13** 44
[13] Yoshihara F, Fuse T, Ao Z, Ashhab S, Kakuyanagi K, Saito S, Aoki T, Koshino K and Semba K 2018 Inversion of qubit energy levels in qubit–oscillator circuits in the deep-strong-coupling regime *Phys. Rev. Lett.* **120** 183601
[14] Bayer A, Pozimski M, Schambeck S, Schuh D, Huber R, Bougeard D and Lange C 2017 Terahertz light–matter interaction beyond unity coupling strength *Nano Lett.* **17** 6340
[15] Frisk Kockum A, Miranowicz A, De Liberato S, Savasta S and Nori F 2019 Ultrastrong coupling between light and matter *Nat. Rev. Phys.* **1** 19
[16] Forn-Díaz P, Lamata L, Rico E, Kono J and Solano E 2019 Ultrastrong coupling regimes of light–matter interaction *Rev. Mod. Phys.* **91** 025005
[17] Ashhab S and Nori F 2010 Qubit–oscillator systems in the ultrastrong-coupling regime and their potential for preparing nonclassical states *Phys. Rev.* A **81** 042311
[18] Rossatto D Z, Villas-Bôas C J, Sanz M and Solano E 2017 Spectral classification of coupling regimes in the quantum Rabi model *Phys. Rev.* A **96** 013849
[19] Facon A, Dietsche E-K, Grosso D, Haroche S, Raimond J-M, Brune M and Gleyzes S 2016 A sensitive electrometer based on a Rydberg atom in a Schrödinger-cat state *Nature* **535** 262
[20] Gheeraert N, Bera S and Florens S 2017 Spontaneous emission of Schrödinger cats in a waveguide at ultrastrong coupling *New J. Phys.* **19** 023036
[21] Leroux C, Govia L C G and Clerk A A 2017 Simple variational ground state and pure-cat-state generation in the quantum Rabi model *Phys. Rev.* A **96** 043834
[22] Gu X, Kockum A F, Miranowicz A, Liu Y-x. and Nori F 2017 Microwave photonics with superconducting quantum circuits *Phys. Rep.* **718–719** 1–102
[23] Beaudoin F, Gambetta J M and Blais A 2011 Dissipation and ultrastrong coupling in circuit QED *Phys. Rev.* A **84** 043832
[24] Ashhab S, Johansson J R and Nori F 2006 Decoherence dynamics of a qubit coupled to a quantum two-level system *Physica* C **444** 45
[25] Nataf P and Ciuti C 2010 Vacuum degeneracy of a circuit QED system in the ultrastrong coupling regime *Phys. Rev. Lett.* **104** 023601
[26] De Liberato S 2017 Virtual photons in the ground state of a dissipative system *Nat. Commun.* **8** 1465
[27] Kwon H, Tan K C, Volkoff T and Jeong H 2019 Nonclassicality as a quantifiable resource for quantum metrology *Phys. Rev. Lett.* **122** 040503
[28] De Bernardis D, Pilar P, Jaako T, De Liberato S and Rabl P 2018 Breakdown of gauge invariance in ultrastrong-coupling cavity QED *Phys. Rev.* A **98** 053819
[29] Di Stefano O, Settineri A, Macrì V, Garziano L, Stassi R, Savasta S and Nori F 2019 Resolution of gauge ambiguities in ultrastrong-coupling cavity quantum electrodynamics *Nat. Phys.* **15** 803
[30] Roth M, Hassler F and DiVincenzo D P 2019 Optimal gauge for the multimode Rabi model in circuit QED *Phys. Rev. Res.* **1** 033128
[31] Stokes A and Nazir A 2019 Gauge ambiguities imply Jaynes–Cummings physics remains valid in ultrastrong coupling QED *Nat. Commun.* **10** 499
[32] Irish E K, Gea-Banacloche J, Martin I and Schwab K C 2005 Dynamics of a two-level system strongly coupled to a high-frequency quantum oscillator *Phys. Rev.* B **72** 195410
[33] Irish E K 2007 Generalized rotating-wave approximation for arbitrarily large coupling *Phys. Rev. Lett.* **99** 173601

[34] Albert V V, Scholes G D and Brumer P 2011 Symmetric rotating-wave approximation for the generalized single-mode spin-boson system *Phys. Rev.* A **84** 042110
[35] Leggett A J, Chakravarty S, Dorsey A T, Fisher M P A, Garg A and Zwerger W 1987 Dynamics of the dissipative two-state system *Rev. Mod. Phys.* **59** 1
[36] Bamba M and Ogawa T 2014 Recipe for the Hamiltonian of system–environment coupling applicable to the ultrastrong-light–matter-interaction regime *Phys. Rev.* A **89** 023817
[37] Zueco D and García-Ripoll J 2019 Ultrastrongly dissipative quantum Rabi model *Phys. Rev.* A **99** 013807
[38] Genoni M G and Paris M G A 2010 Quantifying non-Gaussianity for quantum information *Phys. Rev.* A **82** 052341
[39] Takagi R and Zhuang Q 2018 Convex resource theory of non-Gaussianity *Phys. Rev.* A **97** 062337
[40] Albarelli F, Genoni M G, Matteo G, Paris A and Ferraro A 2018 Resource theory of quantum non-Gaussianity and Wigner negativity *Phys. Rev.* A **98** 052350
[41] Yadin B, Binder F C, Thompson J, Narasimhachar V, Gu M and Kim M S 2018 Operational resource theory of continuous-variable nonclassicality *Phys. Rev.* X **8** 041038
[42] Helstrom C 1968 The minimum variance of estimates in quantum signal detection *IEEE Trans. Inform. Theory* **14** 234
[43] Holevo A S 2011 *Probabilistic and Statistical Aspects of Quantum Theory* (Berlin: Springer)
[44] Nataf P and Ciuti C 2011 Protected quantum computation with multiple resonators in ultrastrong coupling circuit QED *Phys. Rev. Lett.* **107** 190402
[45] Stassi R and Nori F 2018 Long-lasting quantum memories: extending the coherence time of superconducting artificial atoms in the ultrastrong-coupling regime *Phys. Rev.* A **97** 033823
[46] Koshino K, Kono S and Nakamura Y 2020 Protection of a qubit via subradiance: a josephson quantum filter *Phys. Rev. Appl.* **13** 014051
[47] Lolli J, Baksic A, Nagy D, Manucharyan V E and Ciuti C 2015 Ancillary qubit spectroscopy of vacua in cavity and circuit quantum electrodynamics *Phys. Rev. Lett.* **114** 183601
[48] Sánchez Muñoz C, Nori F and De Liberato S 2018 Resolution of superluminal signalling in non-perturbative cavity quantum electrodynamics *Nat. Commun.* **9** 1924
[49] Bera S, Nazir A, Chin A W, Baranger H U and Florens S 2014 Generalized multipolaron expansion for the spin-boson model: environmental entanglement and the biased two-state system *Phys. Rev.* B **90** 075110
[50] Parra-Rodriguez A, Rico E, Solano E and Egusquiza I L 2018 Quantum networks in divergence-free circuit QED *Quantum Sci. Technol.* **3** 024012
[51] Martinazzo R, Vacchini B, Hughes K H and Burghardt I 2011 Communication: universal Markovian reduction of Brownian particle dynamics *J. Chem. Phys.* **134** 011101